Cascade-Zero123: One Image to Highly Consistent 3D with Self-Prompted Nearby Views

Yabo Chen[1]*, Jiemin Fang[2]*, Yuyang Huang[1], Taoran Yi[3], Xiaopeng Zhang[2],
Lingxi Xie[2], Xinggang Wang[3], Wenrui Dai[1], Hongkai Xiong[4], Qi Tian[2]

[1]Department of Computer Science and Engineering, Shanghai Jiao Tong University
[2]Huawei Inc.
[3]Huazhong University of Science and Technology
[4]Department of Electronic Engineering, Shanghai Jiao Tong University

{chenyabo, huangyuyang, daiwenrui, xionghongkai}@sjtu.edu.cn
{jaminfong, 198808xc, zxphistory}@gmail.com {taoranyi, xgwang}@hust.com
tian.qi1@huawei.com
cascadezero123.github.io

Figure 1. Rather than adopting the one-to-one generation pipeline as in Zero-1-to-3 [29], Cascade-Zero123 progressively extracts the 3D information from one single image via self-prompted nearby views. View-consistent images can be generated by constructing the structure in a cascade manner. Cascade-Zero123 shows strong capability on various complex objects, *e.g.* insects, robots, or multiple objects stacked.

Abstract

Synthesizing multi-view 3D from one single image is a significant and challenging task. For this goal, Zero-1-to-3 methods aim to extend a 2D latent diffusion model to the 3D scope. These approaches generate the target-view image with a single-view source image and the camera pose as condition information. However, the one-to-one manner adopted in Zero-1-to-3 incurs challenges for building geometric and visual consistency across views, especially

*Equal contributions.

1

for complex objects. We propose a cascade generation framework constructed with two Zero-1-to-3 models, named Cascade-Zero123, to tackle this issue, which progressively extracts 3D information from the source image. Specifically, a self-prompting mechanism is designed to generate several nearby views at first. These views are then fed into the second-stage model along with the source image as generation conditions. With self-prompted multiple views as the supplementary information, our Cascade-Zero123 generates more highly consistent novel-view images than Zero-1-to-3. The promotion is significant for various complex and challenging scenes, involving insects, humans, transparent objects, and stacked multiple objects etc.

1. Introduction

Large latent diffusion models have achieved remarkable performance in synthesizing high-quality 2D images with significant zero-shot capability [37, 44, 46, 48]. To migrate such generalizability to the 3D field, many researchers have attempted to adapt diffusion models to 3D tasks [1, 5, 8, 12–14, 18, 20, 23, 26, 30, 33, 35, 36, 38, 42, 49, 54, 55, 57–59, 62, 65, 69, 71]. Generating the 3D object from a single image has become an emerging research topic in 3D computer vision, for its flexibility and convenience of various real-world applications [40, 45] including virtual reality, 3D content creation, computer gaming, movie or animation rendering, *etc*.

Regarding the task of using a single image to generate 3D, there are two main research directions. The first is to directly train a 3D model [4, 21, 22, 38, 63], but due to the significant resources required for collecting and organizing 3D data, large-scale 3D datasets are limited. As a result, methods that directly train 3D models perform well only on scenes similar to the training set and lack generalization ability. The second direction focuses on effectively utilizing the 2D latent diffusion, the highlight is to leverage the zero-shot generalization capability obtained from pre-training on large-scale 2D datasets. Models such as Zero-1-to-3 [29] are view-conditioned large latent diffusion models, in which the pre-training of multi-view images based on angle conditioning enables the models to have the ability to reconstruct the structure of unseen samples. For each input image, these models can directly output the corresponding novel-view images. However, the prior 2D diffusion models and view-conditioned latent diffusion models usually generate each image separately. As a result, **the generated images are hard to be geometrically and visually consistent across different views**. How to better utilize the capabilities of view-conditioned latent diffusion models and improve these pre-trained models to perform better novel view synthesis becomes a worthy explored direction.

In practice, for objects with simple structures, *e.g.* centrally symmetric or left-right symmetric objects, Zero-1-to-3 demonstrates excellent 3D cognitive ability and generates consistent novel views. However, for objects with complex structures, **it is challenging to synthesize high-quality novel-view images when the camera pose changes dramatically and incurs completely unseen parts**.

Considering the above issues, we propose a framework, named Cascade-Zero123, to reduce the difficulty of the task, which allows Zero-1-to-3 to progressively extract 3D information from a single image based on the self-prompted nearby views. Cascade-Zero123 consists of two cascade Zero-1-to-3 models called Base-0123 and Refiner-0123. First, we use Base-0123 to generate a set of nearby views, allowing the model to develop a basic 3D prior knowledge of the object. These self-prompt views are then used as condition images and inputted to Refiner-0123. Our pipeline decomposes the task of directly rotating an image to a large rotation angle. Instead, it transforms the task into two parts, which are generating multiple nearby images from the input image and utilizing them as prompts to generate the final target views. As shown in Fig. 2, due to the context cross-attention between multi-view self-prompted condition images and the noise latent in the second Zero-1-to-3, the model's output of multi-view images gains a certain level of geometric and visual consistency.

Our contributions can be summarized as follows:

- We propose a cascade framework to progressively extract 3D information from a single image, preventing directly rotating to completely unseen parts of objects. This can better excavate the novel view synthesis capability of Zero-1-to-3.
- We introduce a self-prompting module that generates multiple nearby viewpoints. With only several multi-view condition images, we can improve the geometric and visual consistency of Zero-1-to-3, which is cheap and effective.
- Our proposed Cascade-Zero123 has better capability to handle complex scenes, even scenarios that were challenging for Zero-1-to-3, such as complex insects, humans, robots, or multiple objects stacked together. Our model has shown evident performance improvements on these previously difficult-to-solve scenes.

2. Related Work

2.1. Single Image to 3D

Many researchers have studied the tasks of generating 3D models and achieving novel view synthesis using only a single image. Some researchers directly train a 3D model on 3D data [4, 21, 22, 38, 63], but they tend to have good generation quality only on scenes similar to the training set.

Recently, by constructing a conditional latent diffusion model based on camera viewpoints, many works made it possible to pre-train a single image-to-3D model [15, 17,

27–29, 31, 32, 34, 43, 50–53, 56, 60, 61, 64, 66, 67]. Zero-1-to-3 [29] learns from large-scale multi-view images [10] to build the geometric priors of large-scale diffusion models. Zero-1-to-3 can lift various images that training sets have never been seen before to 3D with good quality. After that, many works have utilized Zero-1-to-3 as a module to enhance the quality of meshes or 3D models. Magic123 [43] combines the capabilities of Zero-1-to-3 and stable diffusion together to generate 3D models. One-2-3-45 [28] also leverages Zero-1-to-3 to generate different views to assist in mesh generation. However, these methods simply used it as a pre-trained 3D diffusion model tool with fixed checkpoints.

There have also been efforts to improve Zero-1-to-3. Approaches like Consistent1-to-3 [67], and SyncDreamer [31] aim to enhance the consistency of view generation by introducing priors during the denoising process in view-conditioned diffusion models. However, they add models like additional Transformers to render new views which will result in poor generalization due to these additional model's capability, especially when facing unseen single images, so they may not integrate well with generalized latent diffusion models. In addition, the training of additional models usually costs a lot.

Therefore, we argue that Zero-1-to-3 itself has the ability to provide 3D priors and establish 3D consistency, albeit requiring a progressive manner to achieve it. By using self-prompted condition images, Zero-1-to-3 can generate images of higher quality and higher consistency while also maintaining its strong open-set generalization capabilities brought by the large-scale latent diffusion model.

2.2. Multi-stage Diffusion Models

Cascade networks have been widely used in boosting the performance of models in the computer vision field, such as cascade RCNN [2], cascade DETR [68], and so on [24, 25]. After large-scale latent diffusion models became popular, many influential works also used cascade networks to improve the generation quality of models. For example, DeepFloyd-IF [47] achieved high-resolution and high-detail image generation by constructing three cascade pixel diffusion modules: a base model that generates a 64×64 pixel image based on text prompts, and two super-resolution models. Furthermore, SDXL [41] used a cascade structure, in which a base model aligned with a refiner in the latent space to generate higher-quality and higher-resolution images. I2VGen-XL [70] also employed cascade diffusion models to enhance the quality of video generation. However, in the field of single image to 3D, there haven't been works that utilize cascade structure to improve the quality of 3D generation. How to use cascade networks to build 3D consistency and improve 3D model generation quality has become an unsolved problem.

3. Methods

We present the Cascade-Zero123 approach from the following aspects. First, we briefly review the framework of Zero-1-to-3 [29] in Sec. 3.1. Then, we explain how we construct the cascade structure of Zero-1-to-3 in Sec. 3.2. Next, we discuss the design of Base-0123 in Sec. 3.3 and Refiner-0123 to use self-prompted views in Sec. 3.4. Finally, we describe the self-distillation design in Sec. 3.5 and the inference process of the model in Sec. 3.6.

3.1. Preliminary

We first give a brief introduction to diffusion models [11]. The diffusion model's forward process adds the Gaussian noise $\mathcal{N}(\mathbf{0}, \mathbf{I})$, which can be defined as:

$$q\left(x^t \mid x^{t-1}\right) = \mathcal{N}\left(x^t; \sqrt{\alpha_t} x^{t-1}, (1 - \alpha_t)\,\mathbf{I}\right) \quad (1)$$

where α is a scheduling hyper-parameter and $t \in [1, 1000]$ denotes the diffusion timestep. $q\left(x^t \mid x^{t-1}\right)$ is the probability of estimating x^t using x^{t-1}, and $\mathbf{I}$ is the normally distributed variance.

Zero-1-to-3 [29] proposes a latent diffusion model to learn the relationship between the source image x_c and target image x_t during the denoising process, which can be simply defined as:

$$x_t = f_\phi(x_c, \Delta R^{ct}, \Delta T^{ct}). \quad (2)$$

The Zero-1-to-3 model takes an image x_c and the relative camera pose $(\Delta R^{ct}, \Delta T^{ct})$ as the condition. For simplicity, we use Δ to represent the pose transition, including the relative angle rotation and translation from the condition view (R^c, T^c) to the target view (R^t, T^t), i.e. $(\Delta R^{ct}, \Delta T^{ct}) = (R^t, T^t) \ominus (R^c, T^c)$, where $\ominus$ is the pose transition in the corresponding world coordinate and R and T represent the rotation and translation matrix of the camera pose respectively. Specifically, the pose transition computation of the Objaverse dataset coordinate [9, 10] can be found in the appendix.

Using a latent diffusion model with an encoder f_ϕ, a denoiser U-Net ϵ_θ and a decoder $\mathcal{D}$, the denoising process can be defined as follows.

$$\begin{aligned}
p\left(x^{t-1} \mid x^t, c\left(x_c, \Delta R^{ct}, \Delta T^{ct}\right)\right) \\
= \mathcal{N}\left(x^{t-1}; \mu_\theta\left(x^t, t, c\left(x_c, \Delta R^{ct}, \Delta T^{ct}\right)\right),\right. \\
\left. \Sigma_\theta\left(x^t, t, c\left(x_c, \Delta R^{ct}, \Delta T^{ct}\right)\right)\right).
\end{aligned} \quad (3)$$

where $c\left(x_c, \Delta R^{ct}, \Delta T^{ct}\right)$ represents the embedding encoded from the condition image and relative camera pose and the mean distribution μ_θ and variance function Σ_θ is modeled by the denoising U-Net.

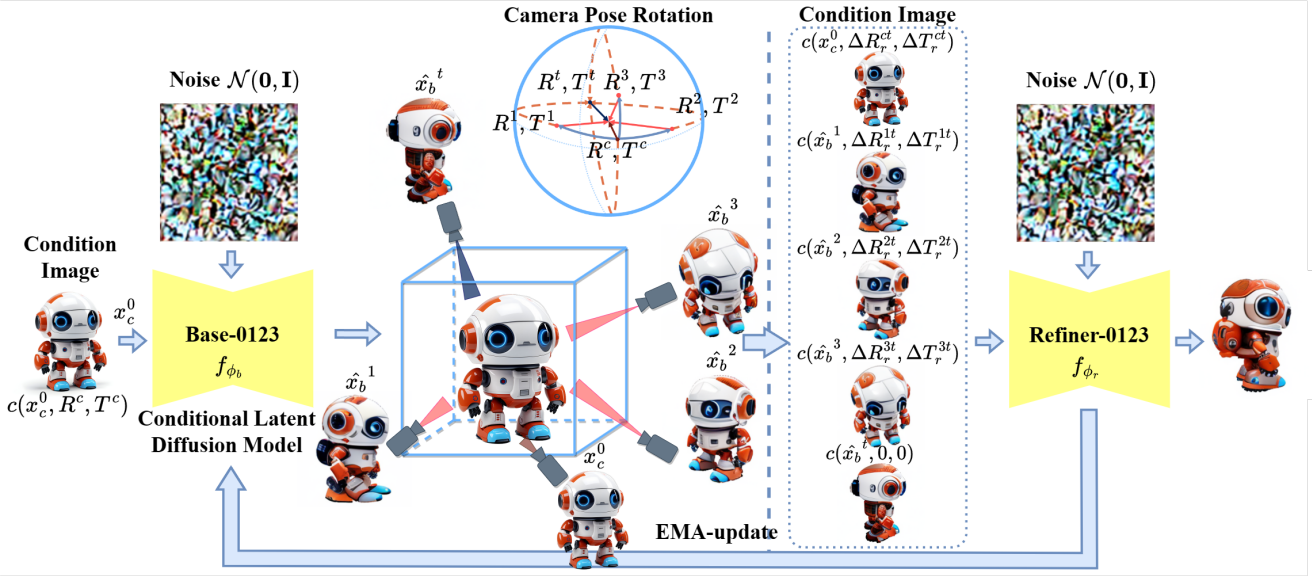At the diffusion time step t, Zero-1-to-3 encodes the embedding of the input view and relative camera pose as

Figure 2. The architecture of Cascade-Zero123. Cascade-Zero123 can be divided into two parts. The left part is Base-0123, which takes a set of R and T values as input to generate corresponding multi-view images. These output images are concatenated with the input condition image and its corresponding camera pose, forming a self-prompted input denoted as a set of $c(x_c, \Delta R, \Delta T)$ for the right part Refiner-0123. The corresponding camera pose transition for each condition image to the target image needs to be recalculated as shown in detailed camera pose rotations. After each iteration of training, Base-0123 is updated through exponential moving average(EMA) using Refiner-0123.

$c(x_c, \Delta R^{ct}, \Delta T^{ct})$ and set the objective loss function as

$$
\begin{aligned}
L(\theta) = \min_{\theta} \mathbb{E}_{z \sim \mathcal{E}(x), t, \epsilon \sim \mathcal{N}(0,1)} \\
\left\| \epsilon - \epsilon_{\theta} \left(z_t, t, c\left(x_c, \Delta R^{ct}, \Delta T^{ct}\right)\right) \right\|_2^2,
\end{aligned}
\tag{4}
$$

where ϵ is the noise prediction corresponding to the distribution. With the model ϵ_{θ} trained, the inference model f_{ϕ} can generate an image by denoising the Gaussian noise conditioned on the embedding of $c(x_c, \Delta R^{ct}, \Delta T^{ct})$.

3.2. Cascade-Zero123 Framework

Modeling the view rotation from a completely unseen image to a large rotation angle is highly challenging for Zero-1-to-3 [29]. We ease this task with a cascade structure, which progressively moves the camera pose with slight changes.

As shown in Fig. 2. Cascade-Zero123 consists of two cascade Zero-1-to-3 models. The first Zero-1-to-3 is referred to as Base-0123, and the second one is referred to as Refiner-0123. In terms of the structure, Base-0123 is responsible for generating multi-view images. Although these images lack consistency, they serve as rough condition inputs, which, along with their corresponding camera poses, are fed into the network of the Refiner-0123 model. The Refiner-0123 is aware of the multi-view input and it will compute the rotation and translation of different viewpoints to the final target view, which can enhance geometric and visual consistency in the outputs. After that, the training

framework incorporates the model parameters of the second Refiner-0123 model back into the Base-0123 through exponential moving average (EMA).

Compared with Eq. 2, we can formulate the proposed Cascade-Zero123 as

$$
\begin{aligned}
x_T = f_{\phi_r}((x_c^0, f_{\phi_b}(x, \Delta R_b^{c\{1:P\}}, \Delta T_b^{c\{1:P\}})), \\
\Delta R_r^{\{1:P\}t}, \Delta T_r^{\{1:P\}t}),
\end{aligned}
\tag{5}
$$

where f_{ϕ_b} and f_{ϕ_r} are the Base-0123 and Refiner-0123 respectively, and the parameters of f_{ϕ_b} can be denoted as ϕ_b and those parameters of f_{ϕ_r} can be denoted as ϕ_r. x_T is the final target image. P is the number of the prompt views, $\Delta R_r^{it}, \Delta T_r^{it}$ is the prompted views camera pose of Refiner-0123.

3.3. Base-0123 Framework

In particular, at the beginning of the pre-training process, a set of input images denoted as x_c^0 is provided to Base-0123. Then we sample some rotation and translation matrices from the nearby viewpoints of the input view, which we denote as $\{(R^i, T^i) | i \in [1, P]\}$, where P is the total number of prompt nearby views. We set the poses of P viewpoints as constant ones to avoid the gap between the training and inference phases.

Our ablation experiments have also demonstrated that generating prompt images with small angles produces good multi-view consistency and final performance. Detailed

4

view setting and hyper-parameter selection can be found in the implementation details of Sec. 4.2.

All the P prompted viewpoints attended with the target view pose (R_t, T_t) are concatenated with the same input embedding as $c\left(x_c^0, \Delta R_b^{ci}, \Delta T_b^{ci}\right), i \in [1, P]$. Specifically, we calculate

$$(\Delta R_b^{ci}, \Delta T_b^{ci}) = (R^i, T^i) \ominus (R^c, T^c) \ i \in [1, P] \quad (6)$$

where $\ominus$ are the pose transitions in the corresponding world coordinate. In this stage, all these poses are drawn as target views. They are fed into the first Base-0123 f_ϕ in parallel.

Compared with Eq. 2, we can formulate the Base-0123 framework as:

$$\begin{aligned}
\{\hat{x}_t^1, \hat{x}_t^2, ..., \hat{x}_t^P\} = & \{f_{\phi_b}(x_c^0, \Delta R_b^{c1}, \Delta T_b^{c1}), \\
& f_{\phi_b}(x_c^0, \Delta R_b^{c2}, \Delta T_b^{c2}), ... \quad (7) \\
& f_{\phi_b}(x_c^0, \Delta R_b^{cP}, \Delta T_b^{cP})\}
\end{aligned}$$

where $\{\hat{x}_t^1, \hat{x}_t^2, ..., \hat{x}_t^P\}$ are exactly self-prompted views.

3.4. Refiner-0123 Framework

After obtaining the multi-view images generated by the first-stage Base-0123 and their corresponding camera poses, we proceed to compute the camera pose rotation changes for each of these images with respect to the final target image. Specifically, we calculate the relative pose transition from self-prompted views to the target views as:

$$(\Delta R_r^{it}, \Delta T_r^{it}) = (R^t, T^t) \ominus (R^i, T^i) \ i \in [1, P] \quad (8)$$

where $\ominus$ are the pose transitions in the corresponding world coordinate, and (R_r, T_r) is the camera pose of the target image. Because the camera rotation and translation from the target view to itself are zero and the rotation of the input view remains the same, i.e. $(\Delta R_r^{tt}, \Delta T_r^{tt}) = (0,0)$, $(\Delta R_r^{ct}, \Delta T_r^{ct}) = (\Delta R_c^{ct}, \Delta T_c^{ct})$ Then as shown in Fig. 2. The second Refiner-0123 takes the input images and self-prompted nearby views $\{\hat{x}_t^1, \hat{x}_t^2, ..., \hat{x}_t^P\}$ as input. Compared with Eq. 2, we can formulate the Refiner-0123 framework as:

$$\begin{aligned}
x_T = & f_{\phi_r}((x_c^0, \Delta R_r^{ct}, \Delta T_r^{ct}), (\hat{x}_t^1, \Delta R_r^{1t}, \Delta T_r^{1t}), ... \\
& (\hat{x}_t^P, \Delta R_r^{Pt}, \Delta T_r^{Pt}), (\hat{x}_t^t, \Delta R_r^{tt}, \Delta T_r^{tt})) \quad (9)
\end{aligned}$$

Reviewing that the conditional denoising autoencoder can control the synthesis process through inputs context y such as text, semantic maps or images [46], the latent diffusion models use attention-based models. The context cross-attention can be formulated as:

$$\text{Attention}(Q, K, V) = \text{softmax}\left(\frac{QK^T}{\sqrt{d}}\right) \cdot V \quad (10)$$

$$Q = W_Q^{(i)} \cdot \varphi_i(z_t), K = W_K^{(i)} \cdot \tau_{\phi_r}(y), V = W_V^{(i)} \cdot \tau_{\phi_r}(y) \quad (11)$$

Here, $\varphi_i(z_t) \in \mathbb{R}^{N \times d_\epsilon^i}$ denotes a (flattened) intermediate representation of the UNet implementing ϵ_{ϕ_r} and $W_V^{(i)} \in \mathbb{R}^{d \times d_\epsilon^i}, W_Q^{(i)} \in \mathbb{R}^{d \times d_\tau}$ and $W_K^{(i)} \in \mathbb{R}^{d \times d_\tau}$ are learnable projection matrices. All prompt views are concatenated through the token dimension so that all these conditions are set as the context of the input $\tau_{\phi_r}(y)$, all conditional embeddings can calculate cross attention to the flattened intermediate representation ϵ_{ϕ_r}.

Then, the objective loss function of the Refiner-0123 model can be set as:

$$\begin{aligned}
\min_\theta & \mathbb{E}_{z \sim \mathcal{E}(x), t, \epsilon \sim \mathcal{N}(0,1)} \| \epsilon - \\
& \epsilon_{\phi_r}\left(z_r, t, c(x_c^0, \hat{x}_t^{\{1:p\}}, \Delta R_r^{\{1:p\}}, \Delta T_r^{\{1:p\}})\right) \|_2^2.
\end{aligned} \quad (12)$$

After the model ϵ_{ϕ_r} is trained, we can get the Refiner-0123 model f_{ϕ_r}.

3.5. Self-Distillation Design

Considering that the Refiner-0123 network f_{ϕ_r} is trained via back-propagation to minimize the denoising loss. Inspired by the methods [3, 6, 7, 16] in the self-supervised learning field. The Base-0123 network is updated in a momentum update way using exponential moving average (EMA). Specifically, we have denoted the parameters of f_{ϕ_b} as ϕ_b and those of f_{ϕ_r} as ϕ_r we update ϕ_b by

$$\phi_b \leftarrow \eta \cdot \phi_b + (1 - \eta) \cdot \phi_r, \quad (13)$$

where $\eta \in [0, 1)$ is a momentum coefficient to control the magnitude decay of updates from the Refiner-0123 to the Base-0123.

3.6. Inference

During the inference stage, given an input image, we need to go through two stages of the DDIM (Denoising Diffusion Probabilistic Model) [19] schedule while simultaneously passing the input image through both the Base-0123 and Refiner-0123 networks.

These views along with their corresponding camera pose rotation and translation differences, are concatenated and input into the Refiner-0123. After computing cross-attention with the context and inputs, another DDIM sampling is performed, generating the final target image.

For the generation from a single image to 3D, the incurred cost is quite similar to the original Zero-1-to-3. Refiner-0123 leverages these condition images to calculate the SDS loss without repeatedly invoking the denoising process of Base-0123. The process is similar to novel view synthesis, but the Base-0123 only needs to be processed once. All the self-prompted nearby views along with the input views are used as condition images and fed into the Refiner-0123 network for computing Score Distillation Sampling (SDS) [42] loss.

4. Experiments

We assess our model's performance on novel view synthesis and single-image to 3D reconstruction tasks. We introduce the datasets, implementation details and metrics from Sec.4.1 to Sec.4.3. And show qualitative results, quantitative results, and ablation studies from Sec.4.4 to Sec.4.6

4.1. Datasets

Objaverse Dataset is a large-scale dataset containing 800K+ annotated 3D mesh objects [39]. We use this dataset for training and validation. We render 12 images per object from uniformly distributed viewpoints surrounding the object, followed by Zero-1-to-3.

Realfusion15 Realfusion15 is the dataset collected and released by RealFusion [34], consisting of 15 natural images that include bananas, birds, cacti, barbie cakes, cat statues, teapots, microphones, dragon statues, fishes, cherries, and watercolor paintings, etc.

4.2. Implementation Details

We train Cascade-Zero123 on the Objaverse dataset [10] which contains about 800k objects. Following Zero-1-to-3, the number of viewpoints rendered is 12. Following the assumption of Zero-1-to-3, we also assume that the azimuth of both the input view and the first target view is $0°$. We train the Cascade-Zero123 for 170k steps with 8 V100 GPUs using a total batch size of 96.

Both Base-0123 and Refiner-0123 load the pre-trained Zero123-XL model initially. In Base-0123, to avoid increasing the pretraining costs, we perform only 25 iterations of DDIM (Differentiable Diffusion Model) for inference on each input view of the object during the pretraining phase. Multiple nearby views share the same input view but concatenate with different camera poses. In Refiner-0123, we choose nearby views of azimuth rotations of $45°$ and $-45°$, a view of elevation rotations of 30 degrees, and the target view generated in the first stage is also set as inputs to Refiner-0123. More details about the selection of nearby views can be found in the ablation studies.

4.3. Metrics

We use the following evaluation metrics to quantitatively evaluate the performance of our model. We first report the Peak Signal-to-Noise Ratio (PSNR). Perceptual Loss (LPIPS) measures the perceptual distance between two images by comparing the deep features extracted by deep neural networks given each image as input. Structural Similarity (SSIM) measures the structural similarity between two images considering both color and texture information. The CLIP-score quantifies the average CLIP distance between the rendered image and the reference image, serving as a measure of 3D consistency by assessing appearance similarity across novel views and the reference view.

4.4. Qualitative Results

Novel View Synthesis We show qualitative results generated by our Cascade-Zero123 in Fig. 2 and Fig. 3. Our model can generalize well to unseen data. We selected various images from real-world scenes or high-quality scenes generated by Stable Diffusion 2.1 [46] for the experiments on novel view synthesis. These scenes include different kinds of environments and objects. We also tested scenarios involving multiple object stacking (such as stacked donuts) and complex branching structures (such as ladybugs and peeled bananas). The selected example images were deliberately chosen to avoid central symmetry or left-right symmetry, which can pose challenges for generating novel views using conditional latent diffusion models. In the case of these difficult-to-maintain consistency scenes, our Cascade-Zero123 achieved better consistency compared to Zero123-XL and significantly improved image quality compared to SyncDreamer. Note that Zero123-XL is a model pre-trained on Objaverse-XL [9, 10] and has superior generation quality.

Single Image to 3D Using SDS Loss We show qualitative results of a single image to 3D using Dreamfusion's Score Distillation Sampling (SDS) loss [42]. All samples are generated by our Cascade-Zero123 and baseline Zero123-XL in Fig. 4. Firstly, as shown in the upper two rows of Fig. 4, after using SDS loss, Zero-1-to-3 tends to learn the backside as the smooth color of the front side. This is due to the one-to-one sparsely generation pipeline so that the model can only perceive information from the prompt of a single image. As a result, the ears of the fox, the back and hair of Lisa(the woman in yellow), and the back of the dinosaur are all learned as the same color. Additionally, due to the influence of front-facing lighting, the top of the little Batman's head is learned as pure white. However, it should be black, the same as the back. With the correction provided by self-prompted views, we no longer have to speculate the color of the backside from scratch. Instead, we can progressively predict the backside based on the side views. This allows us to better learn the true color consistency of unseen views.

In addition, the proposal of self-prompted views has enhanced the ability of Zero-1-to-3 to model the shapes of multiple objects and occluded objects as shown in the middle of Fig. 4. The shapes of multiple bottles are well preserved, and even the occluded rocket fins can be modeled. Moreover, Zero-1-to-3, when combined with SDS, has difficulty modeling objects with transparency. Zero-1-to-3 sometimes learns the backside of transparent or high-brightness objects as pure white mist-like clouds. However, the multi-view conditioning information prevents the model from lacking information about other sides, avoiding the learning of a pure white plane for the backside and providing 3D information for objects with transparency.

6

Figure 3. Novel view synthesis compared with Zero123-XL [9], and SyncDreamer [31], where Zero123-XL is Zero-1-to-3 pre-trained on Objaverse-XL datasets [9], achieving higher performance. We selected some challenging scenes, including stacked objects, parallel objects, and objects with multiple branches. Zero-1-to-3 exhibits good quality in image generation but lacks consistency in these complex scenes. SyncDreamer, on the other hand, demonstrates good consistency but struggles to maintain good quality in image generation. Our model, however, maintains both quality and consistency in these scenarios.

Table 1. Quantitative results on Objaverse. We evaluate our method on the test split of Objaverse [10].

Methods	↑ PSNR	↑ SSIM	↓ LPIPS	↑ CLIP-Score
Zero123-XL [9, 29]	18.68	0.883	0.189	0.758
Magic123 [43]	18.95	0.882	0.167	0.778
Ours	**21.42**	**0.911**	**0.125**	**0.802**

Table 2. Quantitative results on RealFusion15. Evaluation of novel-view synthesis on the RealFusion15 dataset [34].

Methods	↓ LPIPS	↑ CLIP-Score
RealFusion [34]	0.197	0.735
Make-it-3D [56]	0.119	0.839
Zero-1-to-3 [9, 29]	0.068	0.759
Magic123 [43]	0.062	0.747
Consistent-123 [27]	0.056	0.844
Ours	**0.043**	**0.916**

4.5. Quantitative Results

Following prior research [60], which randomly picked up 100 objects from the Objaverse testset, Since the entire Objaverse test set [10] is quite large, testing all samples would require an excessively long time. Following the approach of Consistent123 [60], we randomly selected a subset of samples from the Objaverse test set for testing. These selected samples have not been seen during the training pro-

cess. Compared with Consistent123 [60], we take a larger number of samples for evaluation (Consistent123 only takes 100 samples). Specifically, we randomly selected 200 samples and then randomly selected an input view and a target view following the same setting as Zero-1-to-3. On the Objaverse test set, we measured the reconstruction per-
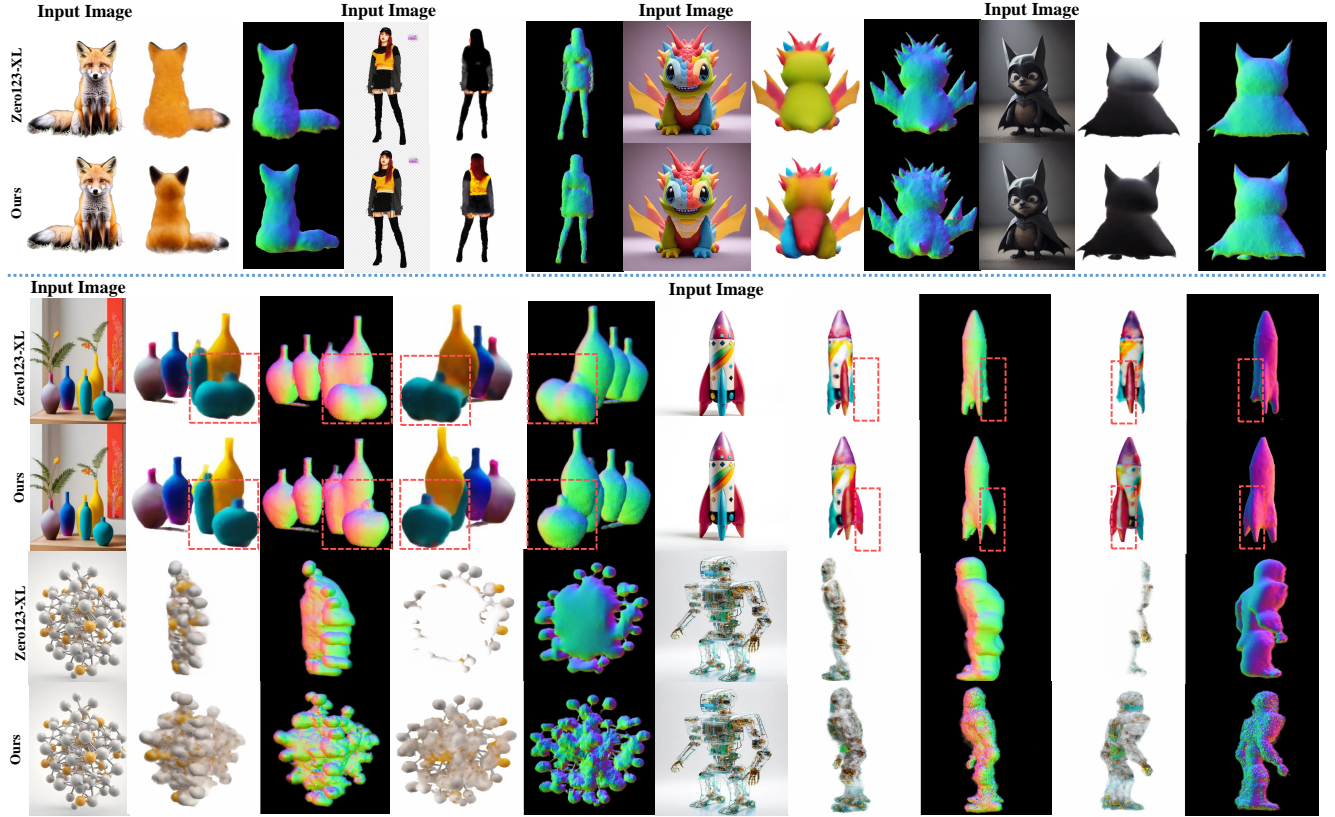
Figure 4. Single image to 3D reconstruction using SDS loss [42] compared with Zero123-XL. The first two rows illustrate that Cascade-Zero123 can correct the problem that the Zero-1-to-3 model sometimes learns inaccurate colors of the backside. The middle two lines describe how Cascade-Zero123 can rectify structural errors in the Zero-1-to-3 model through multi-view self-prompting. The last two lines indicate that Cascade-Zero123 can address the problem of transparent or high-brightness objects being mistakenly learned as white clouds.

Table 3. Ablation studies on the modules of Cascade-Zero123. We evaluate our method on the test split of Objaverse [10].

	↑ PSNR	↓ LPIPS	↑ CLIP-Score
Zero123-XL	18.68	0.189	0.758
+Cascade two Zero-1-to-3 (frozen)	17.67	0.189	0.778
+Prompted random views	18.55	0.179	0.787
+Prompted larger views	19.04	0.172	0.783
+Prompted more nearby views	19.13	0.165	0.789
+Prompted nearby views (Ours)	**20.04**	**0.137**	0.800
-coarse target views	19.99	0.143	0.792
-EMA to Base-0123	19.89	0.139	**0.801**

formance and consistency using metrics of PSNR, SSIM, LPIPS, and CLIP-score. We utilize the checkpoints from Zero123-XL [9, 29]. The index of the selected samples will be made available in the open-source release.

Following Magic123 [43] and Consistent123 [27] We evaluate Cascade-Zero123 against state-of-the-art baselines, including RealFusion [34], Make-it-3D [56], Zero-1-to-3 [29] and Magic123 [43], on the RealFusion15 datasets. Like Magic123, we measure the CLIP-scores and LPIPS which assess the reconstruction quality and visual consistency. As shown in Table. 2, our Cascade-Zero123 surpasses the of state-of-the-art baselines by a lot.

4.6. Ablation Studies

As shown in Table 3, in the ablation study, we provide a detailed explanation for the effectiveness of our method, Cascade-Zero123, based on the following aspects. Firstly we will study whether nearby views perform better than randomly selected views or larger rotated views. Then we will study the impact of having larger rotated prompted condition views. We will also explore the effects of not using the Exponential Moving Average (EMA) and coarse target views. All the experiments presented below were conducted using the same model, pretraining for 120k iterations on 800K samples from the Objaverse dataset. We experiment with the same testing protocol on the Objaverse testset.

Effects of Self-Prompted Structre First, we will validate the difference between incorporating prompted views as inputs to the second-stage model compared to using only the fully trained first-stage model. This analysis will measure the gain achieved by the design of Cascade-Zero123 over the standalone Zero123-XL model. We will then explore various ablations of self-prompted views, including completely random prompted views, denoted as "prompted random views"; inputting images from surrounding viewpoints, specifically inputting images generated by the Base-

0123 at $[90°, 180°, 270°]$ angles as the condition images for the second stage, denoted as "prompted larger views"; and the effects of having more prompted views on the second-stage model. In practice, we selected the azimuth angles of $[-135°, -90°, -45°, 45°, 90°, 135°]$ and elevation angles of $[-10°, 30°]$. We also conduct ablation on the setting of without target views being part of the self-prompted views. Our model results are highlighted in blue.

By simply cascading two Zero-1-to-3 models without training and using self-prompted nearby views, we were able to improve the LPIPS and CLIP scores to some extent, but the PSNR decreased. This validates our hypothesis that using multiple viewpoints as conditions can enhance consistency, but simply cascading them may not work. Secondly, using the same number of random views, larger view degree views or even more views with larger view degree views somewhat do harm to the performance, indicating the need for Zero-1-to-3 to progressively rotate the camera views. Making a large rotation in views at once would lead to large performance degradation.

Effects of Coarse Target Views We also include target views as self-prompted views in our experiments. Incorporating target views and generating coarse target views in advance is also beneficial for novel view synthesis.

Effects of EMA Distillations When the parameters of Base-0123 are not updated and kept fixed, the performance will also degrade. The design of EMA is also shown to have a certain positive effect.

5. Limitation and Conclusion

Limitation Cascade-Zero123 is based on the pre-trained Zero-1-to-3 model [29]. For cases that are extremely difficult for Zero-1-to-3, Cascade-Zero123 has limited ability to handle. The first one lies in the deeply occluded samples. With 2D image input, it is challenging to figure out the exact overlap, so even with nearby views, the overlapping parts may still appear to be stuck together. The 3D depth information will be lost and a flat structure will be potentially learned. Additionally, Zero-1-to-3 is sensitive to camera pose elevation. Therefore, Cascade-Zero123 also struggles with input images that have a high elevation. While our model has already achieved performance and consistency improvement compared to previous models, there are still some potential future directions, *e.g.* enhancing Cascade-Zero123 by incorporating attention between multiple views as [54] and involving multi-modal conditioning information, *e.g.* depth or normal.

Conclusion In this paper, we propose a Cascade-Zero123 network using self-prompted nearby views. Cascade-Zero123 utilizes Zero-1-to-3 as an additional prior constraint, which modifies the one-to-one generation mode of

Zero-1-to-3 and retains the generalized capability as well. With the proposed self-prompted mode, self-prompted views are used as input without the need for additional modules for training. This allows Cascade-Zero123 to improve the geometric and visual consistency of Zero-1-to-3.

References

[1] Mohammadreza Armandpour, Huangjie Zheng, Ali Sadeghian, Amir Sadeghian, and Mingyuan Zhou. Re-imagine the negative prompt algorithm: Transform 2d diffusion into 3d, alleviate janus problem and beyond. *arXiv:2304.04968*, 2023. 2

[2] Zhaowei Cai and Nuno Vasconcelos. Cascade r-cnn: High quality object detection and instance segmentation. *IEEE Transactions on Pattern Analysis and Machine Intelligence*, 2019. 3

[3] Mathilde Caron, Hugo Touvron, Ishan Misra, Hervé Jégou, Julien Mairal, Piotr Bojanowski, and Armand Joulin. Emerging properties in self-supervised vision transformers. In *Proceedings of the International Conference on Computer Vision (ICCV)*, 2021. 5

[4] Eric R. Chan, Koki Nagano, Matthew A. Chan, Alexander W. Bergman, Jeong Joon Park, Axel Levy, Miika Aittala, Shalini De Mello, Tero Karras, and Gordon Wetzstein. GeNVS: Generative novel view synthesis with 3D-aware diffusion models. In *arXiv*, 2023. 2

[5] Rui Chen, Yongwei Chen, Ningxin Jiao, and Kui Jia. Fantasia3d: Disentangling geometry and appearance for high-quality text-to-3d content creation. *arXiv:2303.13873*, 2023. 2

[6] Xinlei Chen, Haoqi Fan, Ross Girshick, and Kaiming He. Improved baselines with momentum contrastive learning. *arXiv*, 2020. 5

[7] Yabo Chen, Yuchen Liu, Dongsheng Jiang, Xiaopeng Zhang, Wenrui Dai, Hongkai Xiong, and Qi Tian. Sdae: Self-distilled masked autoencoder. In *ECCV*, 2022. 5

[8] Zilong Chen, Feng Wang, and Huaping Liu. Text-to-3d using gaussian splatting. *arXiv:2309.16585*, 2023. 2

[9] Matt Deitke, Ruoshi Liu, Matthew Wallingford, Huong Ngo, Oscar Michel, Aditya Kusupati, Alan Fan, Christian Laforte, Vikram Voleti, Samir Yitzhak Gadre, Eli VanderBilt, Aniruddha Kembhavi, Carl Vondrick, Georgia Gkioxari, Kiana Ehsani, Ludwig Schmidt, and Ali Farhadi. Objaverse-xl: A universe of 10m+ 3d objects. *arXiv preprint arXiv:2307.05663*, 2023. 3, 6, 7, 8, 14

[10] Matt Deitke, Dustin Schwenk, Jordi Salvador, Luca Weihs, Oscar Michel, Eli VanderBilt, Ludwig Schmidt, Kiana Ehsani, Aniruddha Kembhavi, and Ali Farhadi. Objaverse: A universe of annotated 3d objects. In *CVPR*, pages 13142–13153, 2023. 3, 6, 7, 8, 13

[11] Dhariwal, Prafulla, , and Alexander Nichol. Diffusion models beat gans on image synthesis. *Advances in neural information processing systems*, 2021. 3

[12] Jiemin Fang, Junjie Wang, Xiaopeng Zhang, Lingxi Xie, and Qi Tian. Gaussianeditor: Editing 3d gaussians delicately

with text instructions. *arXiv preprint arXiv:2311.16037*, 2023. 2

[13] Jun Gao, Tianchang Shen, Zian Wang, Wenzheng Chen, Kangxue Yin, Daiqing Li, Or Litany, Zan Gojcic, and Sanja Fidler. Get3d: A generative model of high quality 3d textured shapes learned from images. *Advances In Neural Information Processing Systems*, 35:31841–31854, 2022.

[14] Anchit Gupta, Wenhan Xiong, Yixin Nie, Ian Jones, and Barlas Oğuz. 3dgen: Triplane latent diffusion for textured mesh generation. *arXiv:2303.05371*, 2023. 2

[15] Abdullah Hamdi, Bernard Ghanem, and Matthias Nießsner. Sparf: Large-scale learning of 3d sparse radiance fields from few input images. In *ICCV*, pages 2930–2940, 2023. 2

[16] Kaiming He, Haoqi Fan, Yuxin Wu, Saining Xie, and Ross Girshick. Momentum contrast for unsupervised visual representation learning. In *CVPR*, pages 9729–9738, 2020. 5

[17] Shoukang Hu, Fangzhou Hong, Tao Hu, Liang Pan, Haiyi Mei, Weiye Xiao, Lei Yang, and Ziwei Liu. Humanliff: Layer-wise 3d human generation with diffusion model. *arXiv:2308.09712*, 2023. 2

[18] Ajay Jain, Ben Mildenhall, Jonathan T Barron, Pieter Abbeel, and Ben Poole. Zero-shot text-guided object generation with dream fields. In *CVPR*, pages 867–876, 2022. 2

[19] Stefano Ermon Jiaming Song, Chenlin Meng. Denoising diffusion implicit models. *ICLR*, 2021. 5

[20] Heewoo Jun and Alex Nichol. Shap-e: Generating conditional 3d implicit functions. *arXiv:2305.02463*, 2023. 2

[21] Heewoo Jun and Alex. et al. Nichol. Shap-e: Generating conditional 3d implicit functions. *arXiv:2305.02463*, 2023. 2

[22] D. Lee, C. Kim, M. Cho, and W. S. Han. Locality-aware generalizable implicit neural representation. In *arXiv:2310.05624*, 2023. 2

[23] Jiabao Lei, Yabin Zhang, Kui Jia, et al. Tango: Text-driven photorealistic and robust 3d stylization via lighting decomposition. *Advances in Neural Information Processing Systems*, 35:30923–30936, 2022. 2

[24] H. Li, B. Shi, W. Dai, Y. Chen, B. Wang, and Y. Sun. Hierarchical graph networks for 3d human pose estimation. *arXiv:2111.11927*, 2021. 3

[25] Ke Li, Shijie Wang, Xiang Zhang, Yifan Xu, Weijian Xu, and Zhuowen Tu. Pose recognition with cascade transformers. 3

[26] Chen-Hsuan Lin, Jun Gao, Luming Tang, Towaki Takikawa, Xiaohui Zeng, Xun Huang, Karsten Kreis, Sanja Fidler, Ming-Yu Liu, and Tsung-Yi Lin. Magic3d: High-resolution text-to-3d content creation. In *CVPR*, pages 300–309, 2023. 2

[27] Yukang Lin, Haonan Han, Chaoqun Gong, Zunnan Xu, Yachao Zhang, and Xiu Li. Consistent123: One image to highly consistent 3d asset using case-aware diffusion priors. *arXiv:2309.17261*, 2023. 3, 7, 8

[28] Minghua Liu, Chao Xu, Haian Jin, Linghao Chen, Zexiang Xu, Hao Su, et al. One-2-3-45: Any single image to 3d mesh in 45 seconds without per-shape optimization. *arXiv:2306.16928*, 2023. 3

[29] Ruoshi Liu, Rundi Wu, Basile Van Hoorick, Pavel Tokmakov, Sergey Zakharov, and Carl Vondrick. Zero-1-to-3: Zero-shot one image to 3d object, 2023. 1, 2, 3, 4, 7, 8, 9, 13, 14

[30] X. Liu, S. H. Kao, J. Chen, Y. W. Tai, and C. K. Tang. Deceptive-nerf: Enhancing nerf reconstruction using pseudo-observations from diffusion models. *arXiv:2305.15171*, 2023. 2

[31] Yuan Liu, Cheng Lin, Zijiao Zeng, Xiaoxiao Long, Lingjie Liu, Taku Komura, and Wenping Wang. Syncdreamer: Generating multiview-consistent images from a single-view image. *arXiv:2309.03453*, 2023. 3, 7, 13, 14

[32] Xiaoxiao Long, Yuan-Chen Guo, Cheng Lin, Yuan Liu, Zhiyang Dou, Lingjie Liu, Yuexin Ma, Song-Hai Zhang, Marc Habermann, Christian Theobalt, et al. Wonder3d: Single image to 3d using cross-domain diffusion. *arXiv:2310.15008*, 2023. 3

[33] Tiange Luo, Chris Rockwell, Honglak Lee, and Justin Johnson. Scalable 3d captioning with pretrained models. *arXiv:2306.07279*, 2023. 2

[34] Luke Melas-Kyriazi, Iro Laina, Christian Rupprecht, and Andrea Vedaldi. Realfusion: 360deg reconstruction of any object from a single image. In *CVPR*, pages 8446–8455, 2023. 3, 6, 7, 8

[35] Oscar Michel, Roi Bar-On, Richard Liu, Sagie Benaim, and Rana Hanocka. Text2mesh: Text-driven neural stylization for meshes. In *CVPR*, pages 13492–13502, 2022. 2

[36] Nasir Mohammad Khalid, Tianhao Xie, Eugene Belilovsky, and Tiberiu Popa. Clip-mesh: Generating textured meshes from text using pretrained image-text models. In *SIGGRAPH Asia 2022 conference papers*, pages 1–8, 2022. 2

[37] Alex Nichol, Prafulla Dhariwal, Aditya Ramesh, Pranav Shyam, Pamela Mishkin, Bob McGrew, Ilya Sutskever, and Mark Chen. Glide: Towards photorealistic image generation and editing with text-guided diffusion models. *arXiv:2112.10741*, 2021. 2

[38] Alex Nichol, Heewoo Jun, Prafulla Dhariwal, Pamela Mishkin, and Mark Chen. Point-e: A system for generating 3d point clouds from complex prompts. *arXiv:2212.08751*, 2022. 2

[39] Yichen Ouyang, Wenhao Chai, Jiayi Ye, Dapeng Tao, Yibing Zhan, and Gaoang Wang. Chasing consistency in text-to-3d generation from a single image. *arXiv:2309.03599*, 2023. 6

[40] A. Paliwal, B. Nguyen, A. Tsarov, and N. K. Kalantari. Reshader: View-dependent highlights for single image view-synthesis. *arXiv:2309.10689*, 2023. 2

[41] D. Podell, Z. English, K. Lacey, A. Blattmann, T. Dockhorn, and J. Müller. Sdxl: Improving latent diffusion models for high-resolution image synthesis. *arXiv:2307.01952*, 2023. 3

[42] Ben Poole, Ajay Jain, Jonathan T. Barron, and Ben Mildenhall. Dreamfusion: Text-to-3d using 2d diffusion. *arXiv*, 2022. 2, 5, 6, 8, 12, 13

[43] Guocheng Qian, Jinjie Mai, Abdullah Hamdi, Jian Ren, Aliaksandr Siarohin, Bing Li, Hsin-Ying Lee, Ivan Skorokhodov, Peter Wonka, Sergey Tulyakov, et al. Magic123: One image to high-quality 3d object generation using both 2d and 3d diffusion priors. *arXiv:2306.17843*, 2023. 3, 7, 8

[44] Aditya Ramesh, Prafulla Dhariwal, Alex Nichol, Casey Chu, and Mark Chen. Hierarchical text-conditional image generation with clip latents. *arXiv:2204.06125*, 2022. 2

[45] B. Roessle, N. Müller, L. Porzi, S. R. Bulò, P. Kontschieder, and M. Nießner. Ganerf: Leveraging discriminators to optimize neural radiance fields. In *arXiv:2306.06044.*, 2023. 2

[46] Robin Rombach, Andreas Blattmann, Dominik Lorenz, Patrick Esser, and Björn Ommer. High-resolution image synthesis with latent diffusion models. In *CVPR*, 2022. 2, 5, 6, 13

[47] C. Saharia, W. Chan, S. Saxena, L. Li, J. Whang, and E. L. Denton. Photorealistic text-to-image diffusion models with deep language understanding. *Advances in Neural Information Processing Systems*, 2022. 3

[48] Chitwan Saharia, William Chan, Saurabh Saxena, Lala Li, Jay Whang, Emily L Denton, Kamyar Ghasemipour, Raphael Gontijo Lopes, Burcu Karagol Ayan, Tim Salimans, et al. Photorealistic text-to-image diffusion models with deep language understanding. *Advances in Neural Information Processing Systems*, 2022. 2

[49] Aditya Sanghi, Hang Chu, Joseph G Lambourne, Ye Wang, Chin-Yi Cheng, Marco Fumero, and Kamal Rahimi Malekshan. Clip-forge: Towards zero-shot text-to-shape generation. In *CVPR*, pages 18603–18613, 2022. 2

[50] Kyle Sargent, Zizhang Li, Tanmay Shah, Charles Herrmann, Hong-Xing Yu, Yunzhi Zhang, Eric Ryan Chan, Dmitry Lagun, Li Fei-Fei, Deqing Sun, et al. Zeronvs: Zero-shot 360-degree view synthesis from a single real image. *arXiv:2310.17994*, 2023. 3

[51] Qiuhong Shen, Xingyi Yang, and Xinchao Wang. Anything-3d: Towards single-view anything reconstruction in the wild. *arXiv:2304.10261*, 2023.

[52] Ruoxi Shi, Hansheng Chen, Zhuoyang Zhang, Minghua Liu, Chao Xu, Xinyue Wei, Linghao Chen, Chong Zeng, and Hao Su. Zero123++: a single image to consistent multi-view diffusion base model. *arXiv:2310.15110*, 2023.

[53] Yukai Shi, Jianan Wang, He Cao, Boshi Tang, Xianbiao Qi, Tianyu Yang, Yukun Huang, Shilong Liu, Lei Zhang, and Heung-Yeung Shum. Toss: High-quality text-guided novel view synthesis from a single image. *arXiv:2310.10644*, 2023. 3

[54] Yichun Shi, Peng Wang, Jianglong Ye, Mai Long, Kejie Li, and Xiao Yang. Mvdream: Multi-view diffusion for 3d generation. *arXiv:2308.16512*, 2023. 2, 9

[55] Jiaxiang Tang, Jiawei Ren, Hang Zhou, Ziwei Liu, and Gang Zeng. Dreamgaussian: Generative gaussian splatting for efficient 3d content creation. *arXiv:2309.16653*, 2023. 2

[56] Junshu Tang, Tengfei Wang, Bo Zhang, Ting Zhang, Ran Yi, Lizhuang Ma, and Dong Chen. Make-it-3d: High-fidelity 3d creation from a single image with diffusion prior. *arXiv:2303.14184*, 2023. 3, 7, 8

[57] Can Wang, Menglei Chai, Mingming He, Dongdong Chen, and Jing Liao. Clip-nerf: Text-and-image driven manipulation of neural radiance fields. In *CVPR*, pages 3835–3844, 2022. 2

[58] Haochen Wang, Xiaodan Du, Jiahao Li, Raymond A Yeh, and Greg Shakhnarovich. Score jacobian chaining: Lifting pretrained 2d diffusion models for 3d generation. In *CVPR*, pages 12619–12629, 2023.

[59] Zhengyi Wang, Cheng Lu, Yikai Wang, Fan Bao, Chongxuan Li, Hang Su, and Jun Zhu. Prolificdreamer: High-fidelity and diverse text-to-3d generation with variational score distillation. *arXiv:2305.16213*, 2023. 2

[60] Haohan Weng, Tianyu Yang, Jianan Wang, Yu Li, Tong Zhang, CL Chen, and Lei Zhang. Consistent123: Improve consistency for one image to 3d object synthesis. *arXiv:2310.08092*, 2023. 3, 7

[61] Zhenzhen Weng, Zeyu Wang, and Serena Yeung. Zeroavatar: Zero-shot 3d avatar generation from a single image. *arXiv:2305.16411*, 2023. 3

[62] Guanjun Wu, Taoran Yi, Jiemin Fang, Lingxi Xie, Xiaopeng Zhang, Wei Wei, Wenyu Liu, Qi Tian, and Wang Xinggang. 4d gaussian splatting for real-time dynamic scene rendering. *arXiv preprint arXiv:2310.08528*, 2023. 2

[63] Jianfeng Xiang, Jiaolong Yang, Binbin Huang, and Xin Tong. 3d-aware image generation using 2d diffusion models. In *Proceedings of the IEEE/CVF International Conference on Computer Vision (ICCV)*, pages 2383–2393, 2023. 2

[64] Dejia Xu, Yifan Jiang, Peihao Wang, Zhiwen Fan, Yi Wang, and Zhangyang Wang. Neurallift-360: Lifting an in-the-wild 2d photo to a 3d object with 360deg views. In *CVPR*, pages 4479–4489, 2023. 3

[65] Jiale Xu, Xintao Wang, Weihao Cheng, Yan-Pei Cao, Ying Shan, Xiaohu Qie, and Shenghua Gao. Dream3d: Zero-shot text-to-3d synthesis using 3d shape prior and text-to-image diffusion models. In *CVPR*, pages 20908–20918, 2023. 2

[66] Jiayu Yang, Ziang Cheng, Yunfei Duan, Pan Ji, and Hongdong Li. Consistnet: Enforcing 3d consistency for multi-view images diffusion. *arXiv:2310.10343*, 2023. 3

[67] Jianglong Ye, Peng Wang, Kejie Li, Yichun Shi, and Heng Wang. Consistent-1-to-3: Consistent image to 3d view synthesis via geometry-aware diffusion models. *arXiv:2310.03020*, 2023. 3

[68] Mingqiao Ye, Lei Ke, Siyuan Li, Yu-Wing Tai, Chi-Keung Tang, Martin Danelljan, and Fisher Yu. Cascade-detr: Delving into high-quality universal object detection. In *ICCV*, 2023. 3

[69] Taoran Yi, Jiemin Fang, Guanjun Wu, Lingxi Xie, Xiaopeng Zhang, Wenyu Liu, Qi Tian, and Xinggang Wang. Gaussiandreamer: Fast generation from text to 3d gaussian splatting with point cloud priors. *arxiv:2310.08529*, 2023. 2

[70] Shiwei* Zhang, Jiayu* Wang, Yingya* Zhang, Kang Zhao, Hangjie Yuan, Zhiwu Qing, Xiang Wang, Deli Zhao, and Jingren Zhou. I2vgen-xl: High-quality image-to-video synthesis via cascaded diffusion models. 2023. 3

[71] Minda Zhao, Chaoyi Zhao, Xinyue Liang, Lincheng Li, Zeng Zhao, Zhipeng Hu, Changjie Fan, and Xin Yu. Efficientdreamer: High-fidelity and robust 3d creation via orthogonal-view diffusion prior. *arXiv:2308.13223*, 2023. 2
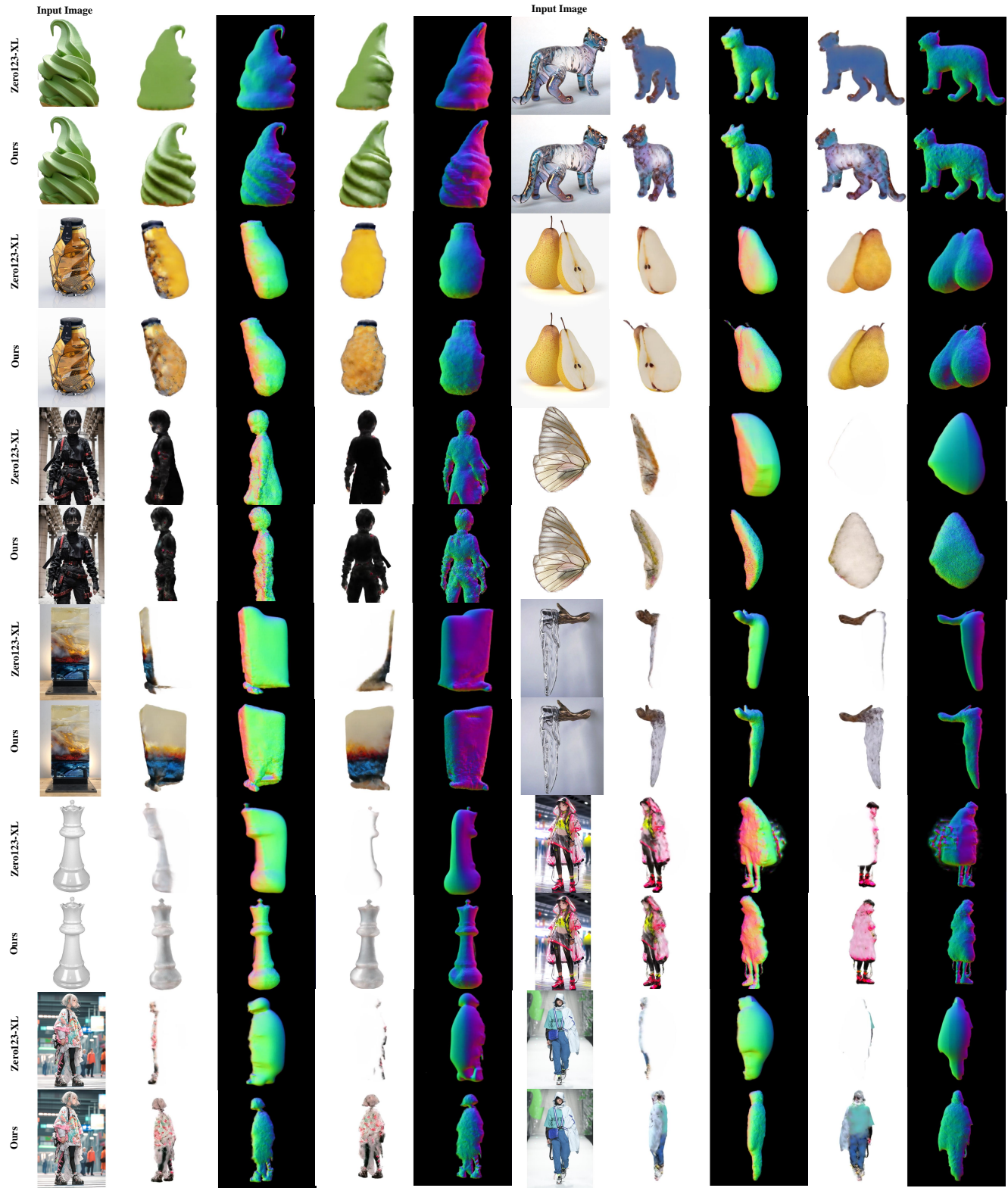
Figure 5. More qualitative results of single image to 3D reconstruction using Dreamfusion SDS loss [42] compared with Zero123-XL. Cascade-Zero123 can correct the backside through multi-view self-prompting, and can also address the problem of transparent or high-brightness objects being mistakenly learned as white clouds.

12

A. Appendix

A.1. More Qualitative Results of Single Image to 3D

We show more qualitative results of the single image to 3D using Dreamfusion's Score Distillation Sampling (SDS) loss [42]. All samples are generated by our Cascade-Zero123 and baseline Zero123-XL in Fig. 5. As shown in the figure, Cascade-Zero123 is able to correct structural and textural errors, as well as the backside errors of objects. For example, the first row of the figure shows that Cascade-Zero123 fixes the texture and structure errors on the back-side of the ice cream. And Cascade-Zero123 correct the color of the backside of the pears and the structure of the pear pedicle at the same time. With the correction provided by self-prompted views, we no longer have to speculate the color of the backside from scratch. Instead, we can progressively predict the backside based on the side views. This allows us to better learn the true color consistency of unseen views.

We also provide qualitative results of multi-view conditioning information that can prevent the incorrect model of transparent objects or objects with high brightness. Our methods avoid learning a pure white plane for the backside and provide more accurate 3D information for these objects. For example, the butterfly wings and the icicle have been learned as solid blocks instead.

A.2. More Qualitative Results of Novel View Synthesis

We show more qualitative results generated by our Cascade-Zero123 in Fig. 6. Our model can generalize well to unseen data. We selected more various images from real-world scenes or high-quality scenes generated by Stable Diffusion 2.1 [46] for the experiments on novel view synthesis. These scenes include different kinds of environments and objects. We tested more scenarios involving multiple object stacking (such as two geese, a computer, and a pumpkin) and complex branching structures (such as a satellite). The selected example images were also deliberately chosen to avoid central symmetry or left-right symmetry, which can pose challenges for generating novel views using conditional latent diffusion models. In the case of these difficult-to-maintain consistency scenes, our Cascade-Zero123 achieved better consistency compared to Zero123-XL and significantly improved image quality compared to SyncDreamer [31]. For SyncDreamer, we choose a variety of elevation angles and random seeds to generate images that try our best to show better performance.

A.3. Cost Analysis

As shown in Table. 4, we compared the pre-training time per iteration between Zero-1-to-3 and our Cascade-Zero123, on the same machine and environment. It can be observed that

Table 4. Cost Analysis of Cascade-Zero123, compared with Zero-1-to-3 [29] The training time of each iteration.

Methods	↓ Pretraining Time
Zero-1-to-3 [29]	9 seconds
Ours	15.7 seconds

our model does not significantly increase the pre-training time. Additionally, during the Single image-to-3D stage, there is only a slight additional inference cost of around a couple of seconds for Base-0123. This extra time can be negligible for single image-to-3D tasks that typically take dozens of minutes.

A.4. The Pose Transition of the Objaverse Dataset Coordinate

The pose transition of the Objaverse dataset [10**?**] coordinate is set as follows:

$$
\begin{cases}
x, y, z & = & R^T \times T \\
\theta & = & arctan(\frac{y}{x}) \\
\phi & = & arctan(\frac{z}{\sqrt{(x^2+y^2)}}) \\
r & = & \sqrt{(x^2 + y^2 + z^2)}
\end{cases}
\tag{14}
$$

where the spherical coordinate θ is the azimuth angle measured in radians from the positive x-axis to the projection, ϕ is the elevation angle defined from the Z-axis down and r is the length of the line from the origin to the camera point). Then $(R^t, T^t) \ominus (R^c, T^c)$ can be formulated in the spherical coordinate as $(\theta_t - \theta_c, \phi_t - \phi_c, r_t - r_c)$.

A.5. Discussion

We will also discuss the possibility of the cascade of view-conditional latent diffusion models in more detail. Models that prioritize consistency and higher quality than Zero-1-to-3 can also benefit from our cascade framework by constructing prompts from multiple views. In our future works, we will experiment with, for example, Cascade SyncDreamer, Cascade Magic123, and Cascade Wonder3D which can also benefit from generating prompts from additional views and cascade structure. Additionally, different types of models can also be cascaded, such as cascading a Consistent123 with Zero123.

Figure 6. More qualitative results of novel view synthesis. Rather than adopting the one-to-one generation pipeline as in Zero-1-to-3 [29], Cascade-Zero123 progressively extracts the 3D information from one single image via self-prompted nearby views. Cascade-Zero123 shows strong capability on different complex objects compared with Zero123-XL [9, 29] and SyncDreamer [31].